




Pauli blocking: probing beyond-mean-field effects in neutrino flavor evolution

Manuel Goimil-García ¹, Shashank Shalgar ¹ and Irene Tamborra ¹

¹*Niels Bohr International Academy & DARK, Niels Bohr Institute,
University of Copenhagen, Blegdamsvej 17, 2100 Copenhagen, Denmark*

(Dated: December 18, 2024)

Neutrino quantum kinetics in dense astrophysical environments is investigated relying on the mean-field approximation. However, it remains to be understood whether mean-field corrections could hinder flavor instabilities that are otherwise foreseen. In this paper, we heuristically explore whether beyond-mean-field effects due to neutrino degeneracy can affect the flavor conversion physics. We find that these corrections shift the stability regions for a suite of (anti)neutrino distributions; a configuration of angular distributions that is stable in the mean-field case can become unstable, or the flavor conversion of previously unstable ensembles can be damped. Our work should serve as a motivation for further understanding the limitations of the mean-field treatment.

I. INTRODUCTION

In a matter background, neutrino flavor evolution can be modified due to the refraction experienced by neutrinos [1–5]. A well-known example of this phenomenon is the Mikheyev-Smirnov-Wolfenstein effect: neutrino refraction on electrons can significantly alter the probability of flavor conversion [1–3]. When the neutrino density is very large, such as in core-collapse supernovae and neutron-star merger remnants, neutrino refraction due to other neutrinos leads to non-linear flavor evolution [4–10]. Neutrino-neutrino refractive effects can make an incoherent mixture of neutrinos unstable [11, 12], with small perturbations in the neutrino flavor states growing exponentially. A defining trait of neutrino self-interaction is that the evolution of all particles in the ensemble is coupled, leading to collective neutrino flavor conversion.

An interesting category of collective effects occurs when the (anti)neutrino momentum distribution is anisotropic. If the angular distributions of ν_e and $\bar{\nu}_e$ are such that the Electron Lepton Number (ELN) of neutrinos changes sign along a specific direction, significant flavor evolution could take place, even in the limit of vanishing vacuum mixing term [13–21]. In this case, the growth rate of flavor coherence is directly proportional to the neutrino density, for which reason these instabilities are named “fast” [22–24].

Fast flavor conversion is expected to occur in the neutrino decoupling regions of core-collapse supernovae and neutron-star merger remnants, with potential implications for the neutrino-driven explosion mechanism and the nucleosynthesis of elements heavier than iron [25–32]. However, our current understanding of collective flavor conversion is based on the solution of neutrino quantum kinetic equations that employ the mean-field approximation [5, 33]. The validity of the mean-field approach and the nature of the resulting phenomenology are the subject of investigation. For example, ongoing work attempts to look for many-body corrections to the mean-field treatment (cf., e.g., Ref. [34] and references therein), but tractable systems are too idealized to give

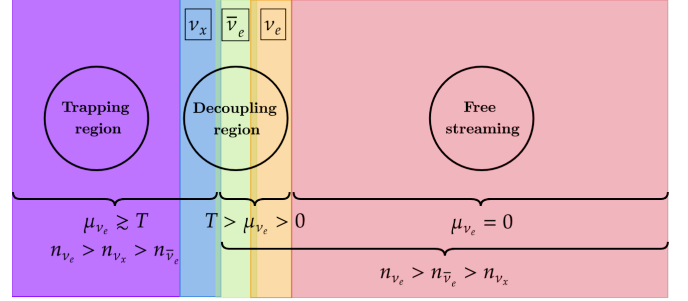


FIG. 1. Sketch of the neutrino decoupling region in the core of compact astrophysical sources. Close to the center, where the chemical potential of electron-flavor neutrinos is the highest, the local neutrino number density is isotropized by collisions with matter, and neutrino flavor conversion is not expected. Moving at larger distances from the source core, the neutrino degeneracy decreases, neutrinos gradually decouple from matter, and flavor instabilities are expected as ELN crossings develop.

an insight on any eventual implications on astrophysical sources [35, 36].

Many-body treatments allow for correlations between particles with different momenta, which are explicitly forbidden at the mean-field level. Such correlations could arise due to entanglement or close to the core of compact astrophysical sources, where the baryon density reaches nuclear levels, and (anti)neutrinos are degenerate and undergo frequent collisions with matter: see the sketch in Fig. 1. Hence, there is reason to ask whether they could lead to novel neutrino flavor instabilities. The region where beyond-mean-field corrections due to neutrino degeneracy could affect flavor evolution can be constrained *a priori*. At nuclear densities, neutrinos of all flavors are in thermal equilibrium with matter because of frequent interactions with the background. The chemical potential for the heavy-lepton flavors (ν_x and $\bar{\nu}_x$) is negligible, and for electron (anti)neutrinos, ν_e ($\bar{\nu}_e$), it is positive (negative). This leads to the following hierarchy between the number densities of the different neutrino species: $n_{\nu_e} > n_{\nu_x} > n_{\bar{\nu}_e}$. Hence, as long as neutrinos

are trapped, flavor instabilities are disfavored. At larger distances from the source core, as the baryon density decreases and neutrino decoupling occurs, $n_{\nu_x} < n_{\nu_e}, n_{\bar{\nu}_e}$; in this region, the (anti)neutrino angular distributions become forward peaked and ELN crossings develop [37–39]. This means that fast flavor instabilities can occur, but momentum correlations are unlikely to have an effect due to low neutrino density. If beyond-mean-field corrections caused by neutrino degeneracy should have an impact on flavor evolution, their effect should originate in the region of transition between the trapping and free-streaming regimes.

In this paper, we explore the impact of beyond-mean-field corrections due to neutrino degeneracy on neutrino quantum kinetics and, in particular, whether flavor instabilities can arise from or be suppressed by these effects. This manuscript is structured as follows. In Sec. II, we provide an overview of the neutrino equations of motion in the presence of neutrino self-interactions and introduce a heuristic prescription aiming to gauge beyond-mean-field effects linked to neutrino degeneracy. In Sec. III, we linearize the neutrino equations of motion and, relying on a toy model, compute the growth rate of flavor instabilities for a set of ELN angular distributions, within the single-energy approximation. In Sec. IV, we present the solutions of the neutrino equations of motion for three benchmark ELN distributions. To understand the flavor evolution in the non-linear regime in the presence of neutrino degeneracy, we compare our results with the well-known case of the fast flavor pendulum [16, 21]. In Sec. V, we relax the single-energy approximation and assess whether the energy dependence further affects the development of flavor instabilities. Finally, we discuss our findings and conclude in Sec. VI.

II. NEUTRINO EQUATIONS OF MOTION

In the mean-field approximation, (anti)neutrinos are described by a set of 2×2 density matrices of the form:

$$\rho_{\mathbf{r},\mathbf{p}} = \begin{pmatrix} \rho_{ee;\mathbf{r},\mathbf{p}} & \rho_{ex;\mathbf{r},\mathbf{p}} \\ \rho_{ex^*;\mathbf{r},\mathbf{p}} & \rho_{xx;\mathbf{r},\mathbf{p}} \end{pmatrix}, \quad (1a)$$

$$\bar{\rho}_{\mathbf{r},\mathbf{p}} = \begin{pmatrix} \bar{\rho}_{ee;\mathbf{r},\mathbf{p}} & \bar{\rho}_{ex;\mathbf{r},\mathbf{p}} \\ \bar{\rho}_{ex^*;\mathbf{r},\mathbf{p}} & \bar{\rho}_{xx;\mathbf{r},\mathbf{p}} \end{pmatrix}, \quad (1b)$$

where $\rho_{l\nu';\mathbf{r},\mathbf{p}}$ and $\bar{\rho}_{l\nu';\mathbf{r},\mathbf{p}}$ denote the number density ($l = l'$) and flavor coherence ($l \neq l'$). These quantities represent an average over a certain volume (momentum spread) around the position \mathbf{r} (momentum \mathbf{p}). Equation (1) carries the assumption that inhomogeneities only occur at large scales, e.g. due to temperature gradients in the medium [5, 33, 40]. Short-range fluctuations would be associated with large momentum uncertainties, which would make it impossible to specify \mathbf{p} . Moreover, in a strongly inhomogeneous system, different momenta would be correlated, so $\rho_{\mathbf{r},\mathbf{p}}$ and $\bar{\rho}_{\mathbf{r},\mathbf{p}}$ cannot fully describe the ensemble [41]. In this section, we first introduce the

equations of motion of neutrinos within the mean-field approximation, and then modify them to take into account effects linked to neutrino degeneracy not included in the mean-field approach.

In the following, we assume that the system is fully axisymmetric and normalize the density matrices such that $(2\pi)^{-1} \int d^3p \text{Tr}(\rho_{\mathbf{p}}) = 1$ and $(2\pi)^{-1} \int d^3p \text{Tr}(\bar{\rho}_{\mathbf{p}}) = \bar{n}_\nu/n_\nu$, where n_ν (\bar{n}_ν) is the total (anti)neutrino number density. A factor 2π from the integral over the azimuthal angle is absorbed into the definition of $\rho_{\mathbf{r},\mathbf{p}}$ and $\bar{\rho}_{\mathbf{r},\mathbf{p}}$, and the momentum distribution can be parametrized in terms of energy, $E = |\mathbf{p}|c$, and radial velocity vc .

A. Equations of motion within the mean-field approximation

The mean-field approximation assumes that, locally, all (anti)neutrinos can be described as plane waves. This approach prevents any correlation between neutrinos with different momenta. Neutrinos with the same flavor are indistinguishable, so their quantum state has to be antisymmetric to particle exchange, and momentum correlations should appear naturally. Hence, $\rho_{\mathbf{r},\mathbf{p}}$ and $\bar{\rho}_{\mathbf{r},\mathbf{p}}$ do not fully describe a quantum state; they determine a phase-space distribution that averages over different particles.

Within this framework, the evolution of the density matrices is driven by coherent forward scattering, i.e. refraction. In particular, if a neutrino can interact with many identical neutrinos, the transition amplitudes of all allowed processes add up coherently. In a homogeneous medium, the interference terms enhance elastic processes such as:

$$\nu_l(\mathbf{p}) + \nu_{l'}(\mathbf{q}) \rightarrow \nu_l(\mathbf{q}) + \nu_{l'}(\mathbf{p}), \quad (2a)$$

$$\nu_l(\mathbf{p}) + \bar{\nu}_{l'}(\mathbf{q}) \rightarrow \nu_{l'}(\mathbf{p}) + \bar{\nu}_l(\mathbf{q}). \quad (2b)$$

These interactions provide the mechanism behind collective flavor conversion, as they can amplify the flavor coherence generated by the neutrino mass difference. Their effect on a purely homogeneous (anti)neutrino ensemble ($\rho_{\mathbf{r},\mathbf{p}} \rightarrow \rho_{\mathbf{p}}$ and $\bar{\rho}_{\mathbf{r},\mathbf{p}} \rightarrow \bar{\rho}_{\mathbf{p}}$) is described by the following Hamiltonian:

$$H_{\mathbf{p}} = \mu \int \frac{d^3p'}{2\pi E'^2} \left(1 - \frac{\mathbf{p} \cdot \mathbf{p}'}{|\mathbf{p}||\mathbf{p}'|} \right) (\rho_{\mathbf{p}'} - \bar{\rho}_{\mathbf{p}'}), \quad (3)$$

where $\mu \equiv \sqrt{2}G_F(\hbar c)^3 n_\nu$ is the neutrino-neutrino interaction strength and n_ν is the total neutrino number density. We note that the mean-field Hamiltonian depends on the direction of the (anti)neutrino trajectory (v), but not on the energy of the particle. Accordingly, the mean-field equations of motion for a homogeneous ensemble can be written as:

$$i\hbar \frac{\partial \rho_{\mathbf{p}}}{\partial t} = \mu([D_0, \rho_{\mathbf{p}}] - v[D_1, \rho_{\mathbf{p}}]), \quad (4a)$$

$$i\hbar \frac{\partial \bar{\rho}_{\mathbf{p}}}{\partial t} = \mu([D_0, \bar{\rho}_{\mathbf{p}}] - v[D_1, \bar{\rho}_{\mathbf{p}}]), \quad (4b)$$

where $D_n \equiv \int d^3p' (2\pi E'^2)^{-1} L_n(v') (\rho_{\mathbf{p}'} - \bar{\rho}_{\mathbf{p}'})$. Here, L_n are the Legendre polynomials, normalized such that $\int_{-1}^{+1} dv' L_n(v') L_m(v') = (n + \frac{1}{2})^{-1}$, and $v'c$ is the radial (anti)neutrino velocity.

The density matrices do not describe an antisymmetric quantum state, but Eqs. (4) cannot violate the exclusion principle. Even if the mean-field framework is extended to include incoherent processes (collisions), which can change the number of particles, the scattering rates tend to 0 as the (anti)neutrino occupation numbers increase [5]. Hence, no momentum mode can have an occupation number greater than 1. However, it is important to question how neglecting momentum correlations shapes our understanding of flavor conversion. For example, it is usually assumed that the system starts as a mixture of pure flavor eigenstates (i.e. the density matrices are diagonal). This is motivated when describing astrophysical environments, where (anti)neutrinos are emitted as highly localized wavepackets with a specific flavor: if these functions do not overlap, then the system is fully incoherent. On the other hand, two plane waves with the same momentum always interfere.

B. Beyond-mean-field effects linked to neutrino degeneracy

If the ensemble is inhomogeneous, the momenta in Eq. (2) are approximate quantities. The interacting particles do not exactly swap their momenta, nor are they scattered precisely in the forward direction. The initial and final momenta are indistinguishable within their uncertainties. In particular, this means that every neutrino contributing to the scattering amplitude can recoil to some extent. This momentum exchange cannot be captured by the mean-field approximation and could modify the development of coherence (see Fig. 2): neutrinos cannot recoil into states that are already occupied, so certain coherent processes could be Pauli blocked, if the neutrino ensemble is degenerate.

As a thought experiment, let us consider a collision between two beams of degenerate neutrinos, one made of ν_e and the other of ν_x . At the mean-field level, the amplitude of $\nu_e \rightarrow \nu_x$ transitions would be the same as that of $\nu_x \rightarrow \nu_e$ processes. However, if momentum exchange is allowed, $\nu_e \rightarrow \nu_x$ should be favored in the first beam, and $\nu_x \rightarrow \nu_e$ in the other. In this case, the description of a coherent neutrino-neutrino interaction would require non-Hermitian operators, as it is done when incoherent scattering is taken into account [5, 42]. We note that the evolution of the system as a whole has to be Hermitian, but not for each momentum mode.

Working out the form of this non-Hermitian Hamiltonian exceeds the scope of this paper. We attempt to assess whether neutrino degeneracy could lead to beyond-mean-field corrections that would affect flavor instabilities. The occurrence of fast instabilities depends on the presence of a crossing in the ELN angular distribu-

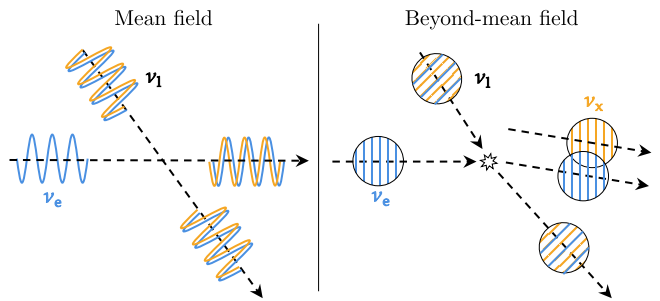


FIG. 2. Neutrino-neutrino interactions in the mean-field approximation (left) vs. beyond-mean-field case (right). In both cases, the incoming ν_e (in blue) is in a flavor eigenstate, and a small seed of flavor coherence is generated by vacuum oscillations (the incoming ν_1 and the outgoing neutrinos are represented as superpositions of ν_e and ν_x eigenstates, with ν_x being plotted in orange). In the mean-field scenario, no momentum is exchanged; the neutrino scatters in the forward direction and its flavor coherence grows as a result. In the beyond-mean-field picture, a small momentum exchange takes place, so the incoming ν_e is scattered onto a region where there already are ν_x 's. The latter do not participate in the interaction, but alter the development of flavor coherence.

tion [15, 43]. However, this requisite can be relaxed, e.g., by effects such as vacuum mixing. The mass difference term in the neutrino dispersion relation can be absorbed into the definition of an effective ELN angular distribution, with stability being determined by crossings in the latter [44]. Likewise, we explore the possibility that momentum correlations in the self-interaction Hamiltonian can be modeled with effective density matrices, $\tilde{\rho}_{\mathbf{p}}$ and $\tilde{\bar{\rho}}_{\mathbf{p}}$.

In order to motivate the form of these effective density matrices, we note that, if all quantum states are filled, no net flavor conversion should take place. Thus, it is reasonable to assume that, within a single-particle framework, any corrections to Eqs. (4) should scale with the (anti)neutrino occupation numbers. Since the expected effect is a flavor-dependent suppression of coherent scattering, we propose the following ansatz:

$$i\hbar \frac{\partial \rho_{\mathbf{p}}}{\partial t} = \mu([\tilde{D}_0, \tilde{\rho}_{\mathbf{p}}] - v[\tilde{D}_1, \tilde{\rho}_{\mathbf{p}}]), \quad (5a)$$

$$i\hbar \frac{\partial \tilde{\bar{\rho}}_{\mathbf{p}}}{\partial t} = \mu([\tilde{D}_0, \tilde{\bar{\rho}}_{\mathbf{p}}] - v[\tilde{D}_1, \tilde{\bar{\rho}}_{\mathbf{p}}]). \quad (5b)$$

Here

$$\tilde{\rho}_{\mathbf{p}} = \begin{pmatrix} [1 - B_{e;\mathbf{p}}]^{1/2} \rho_{ee;\mathbf{p}} & \rho_{ex;\mathbf{p}} \\ \rho_{ex;\mathbf{p}}^* & [1 - B_{x;\mathbf{p}}]^{1/2} \rho_{xx;\mathbf{p}} \end{pmatrix}, \quad (6a)$$

$$\tilde{\bar{\rho}}_{\mathbf{p}} = \begin{pmatrix} [1 - \bar{B}_{e;\mathbf{p}}]^{1/2} \bar{\rho}_{ee;\mathbf{p}} & \bar{\rho}_{ex;\mathbf{p}} \\ \bar{\rho}_{ex;\mathbf{p}}^* & [1 - \bar{B}_{x;\mathbf{p}}]^{1/2} \bar{\rho}_{xx;\mathbf{p}} \end{pmatrix}, \quad (6b)$$

and the effective Hamiltonian is written in terms of $\tilde{D}_n = \int d^3p (2\pi E'^2)^{-1} L_n(v') (\tilde{\rho}_{\mathbf{p}'} - \tilde{\bar{\rho}}_{\mathbf{p}'})$.

The blocking functions B_l (\bar{B}_l) represent the ν_l ($\bar{\nu}_l$)

occupation numbers,

$$B_{l;\mathbf{p}} \equiv \frac{(hc)^3}{2\pi E^2} n_{\nu} \rho_{ll;\mathbf{p}} \text{ and } \bar{B}_{l;\mathbf{p}} \equiv \frac{(hc)^3}{2\pi E^2} n_{\nu} \bar{\rho}_{ll;\mathbf{p}}. \quad (7)$$

When the (anti)neutrino ensemble is in thermal equilibrium with matter, these functions are isotropic, following a Fermi-Dirac distribution:

$$B_{l;E}^{\text{eq}} = \left[\exp\left(\frac{E - \mu_{\nu_l}}{T}\right) + 1 \right]^{-1}, \quad (8a)$$

$$\bar{B}_{l;E}^{\text{eq}} = \left[\exp\left(\frac{E + \mu_{\nu_l}}{T}\right) + 1 \right]^{-1}, \quad (8b)$$

where μ_{ν_l} is the chemical potential of neutrinos with flavor l , and T is the local temperature. The $1/2$ exponent in Eqs. (6) is motivated by the fact that, while neutrino cross sections are suppressed by $\prod_i (1 - B_i)$, it is the scattering amplitude that enters the calculation of the neutrino refractive index.

In the rest of the paper, we investigate the effect of such beyond-mean-field corrections due to neutrino degeneracy. We stress that while the mean-field equations presented in Ref. [5] do take into account Pauli blocking effects, momentum correlations are not considered in the mean-field approach.

III. LINEAR STABILITY ANALYSIS

Given a set of initial conditions $D_{\mathbf{p}}(t=0) = (\rho_{\mathbf{p}} - \bar{\rho}_{\mathbf{p}})(t=0)$, the existence of flavor instabilities can be assessed by linearizing Eqs. (4) and solving the resulting eigenvalue problem, $i\dot{D}_{ex;\mathbf{p}} = \Omega D_{ex;\mathbf{p}}$ [12]. In the single-energy approximation, where $E = |\mathbf{p}|c$ is fixed, the eigenfrequencies Ω are roots of the following polynomial:

$$(I_0 - 1)(I_2 + 1) - I_1^2 = 0, \quad (9)$$

with

$$I_n = \mu \int dv v^n \frac{\tilde{D}_{ee;\mathbf{p}}}{H_{ee;\mathbf{p}} - \Omega}, \quad (10)$$

where $H_{ee;\mathbf{p}} \equiv \tilde{D}_{0,ee} - v\tilde{D}_{1,ee}$ and $D_{xx;\mathbf{p}} = 0$. If $\Omega \in \mathbb{C}$, small perturbations in $D_{ex;\mathbf{p}}$ can grow exponentially at a rate $|\text{Im}(\Omega)|$, and the ensemble undergoes collective flavor conversion.

We solve Eq. (9) for the following family of ELN distributions:

$$\rho_{ee;\mathbf{p}} = \frac{1}{2} \frac{4\pi E^2 B_{e;E}^{\text{eq}}}{(hc)^3 n_{\nu}}, \quad (11a)$$

$$\bar{\rho}_{ee;\mathbf{p}} = \rho_{ee;\mathbf{p}} \left[\frac{\bar{B}_{e;E}^{\text{eq}}}{B_{e;E}^{\text{eq}}} - \frac{F}{2} + \frac{0.2}{d} \exp\left(-\frac{(1-v)^2}{2b^2}\right) \right], \quad (11b)$$

$$\rho_{xx;\mathbf{p}} = \bar{\rho}_{xx;\mathbf{p}} = 0, \quad (11c)$$

where $F = 0.2d^{-1} \int_{-1}^{+1} dv \exp[-(1-v)^2/(2b)^2]$, and d and b are free parameters. The occupation numbers $B_{e;E}^{\text{eq}}$ ($\bar{B}_{e;E}^{\text{eq}}$) explicitly depend on the (anti)neutrino energy, as well as on the thermodynamic properties of the medium. We consider $E = 10.7$ MeV, $T = 10$ MeV, and $\mu_{\nu_e} = 3$ MeV, which may be representative of the $\bar{\nu}_e$ decoupling region in a core-collapse supernova at $\mathcal{O}(0.1)$ s post-bounce. Then, the functionals in Eq. (11) are such that electron neutrinos are isotropically distributed, whereas electron antineutrinos are forward peaked. We vary the parameters entering the angular distributions in the intervals $d \in [0.20, 0.45]$ and $b \in [0.1, 0.8]$, so that our parameter space encompasses both quasi-isotropic ELN distributions and functions with a very deep crossing. Note that the neutrino energy dependence only enters the equations of motion through $B_{e;E}^{\text{eq}}$ and $\bar{B}_{e;E}^{\text{eq}}$, since we focus on fast flavor conversion and therefore the vacuum mixing term in the Hamiltonian is neglected, see Eqs. (5).

Figure 3 displays the growth rate of flavor instability, $\text{Im}(\Omega)/\mu$, for our suite of ELN distributions in the plane spanned by the parameters b and d [see Eq. (11)]. The mean-field (beyond-mean-field) result is shown in the left (right) panel. In particular, we highlight three cases: Case A, corresponding to $(b = 0.40, d = 0.41)$; Case B which has $(b = 0.35, d = 0.33)$; and Case C obtained for $(b = 0.60, d = 0.25)$. These benchmark distributions are plotted in Fig. 4 (dashed lines). The growth rates for the flavor instabilities obtained in the mean-field and beyond-mean-field cases are summarized in Table I for the three selected distributions.

If the equations of motion are modified by beyond-mean field effects due to Pauli blocking (cf. Eq. (5)), the growth rate is suppressed. This is the case for Cases B and C, as shown in Table I. Nevertheless, for ELN distributions on the verge of becoming unstable, these same modifications can lead to a non-zero growth rate, see Case A. These examples also illustrate that the growth rate of the flavor instability is not directly proportional to the depth of the ELN crossing, since $|\text{Im}(\Omega_{\text{BMF}})|$ is larger in Case A than in Case C. Rather, the stable region of our parameter space is determined by the behavior of the integrals I_n defined in Eq. (9), which depend not only on the shape of the crossed region, but also on the total lepton number (D_0) and flux (D_1) [16, 45].

TABLE I. Growth rate of the flavor instability for our three selected angular distributions in Fig. 4, in the mean-field $[\text{Im}(\Omega_{\text{MF}})]$ and beyond-mean-field $[\text{Im}(\Omega_{\text{BMF}})]$ cases.

Distribution	(b, d)	$\text{Im}(\Omega_{\text{MF}}) [\mu]$	$\text{Im}(\Omega_{\text{BMF}}) [\mu]$
Case A	(0.40, 0.41)	0	0.0011
Case B	(0.35, 0.33)	0.0161	0.0108
Case C	(0.60, 0.25)	0.0067	0.0008

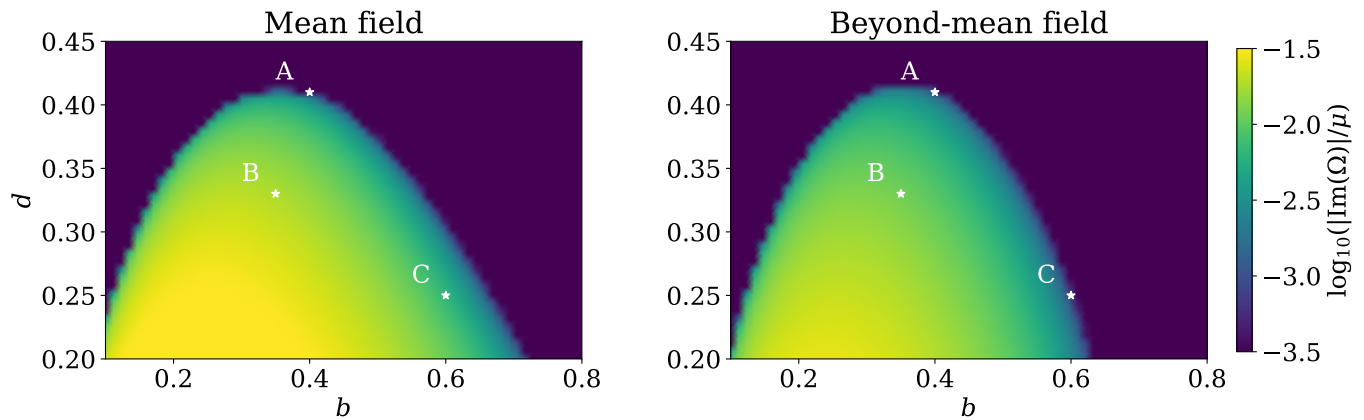


FIG. 3. Contour plot of the growth rate of the flavor instability in the plane spanned by the parameters of the angular distributions b and d , see Eq. (11), in the mean-field scenario (left panel) and for the case taking into account beyond-mean-field corrections due to Pauli blocking (right panel). Our three representative ELN distributions (Cases A, B, and C) are highlighted through the white stars. Overall, the beyond-mean-field prescription changes the stable regions of the ELN parameter space, with the growth rate being suppressed in most cases.

IV. NON-LINEAR FLAVOR EVOLUTION

To assess the effect of the modifications induced by neutrino degeneracy on flavor conversion, we solve Eqs. (5) for the angular distributions in Fig. 4. Instead of generating flavor coherence over time through vacuum mixing, we consider a small off-diagonal perturbation in the off-diagonal terms of the density matrices ($\rho_{ex,\mathbf{p}} = 10^{-6}$ and $\bar{\rho}_{ex,\mathbf{p}} = 10^{-6}$).

Figure 5 shows the angle-integrated neutrino density (left panels) and flavor coherence (right panels), $\rho_{0,ee}$ and $|\rho_{ex}|_0$, for Cases A, B, and C in the mean-field (top pan-

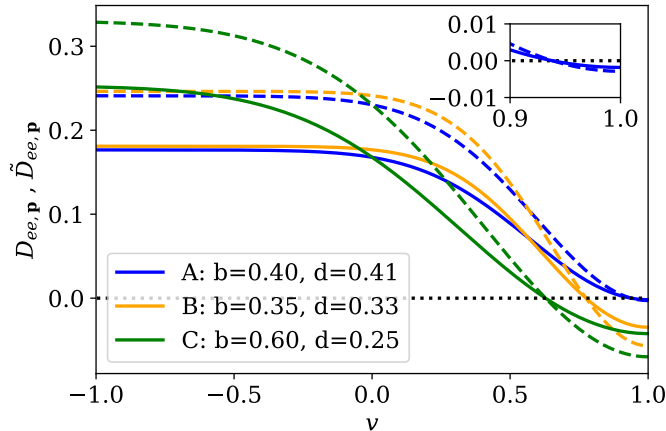


FIG. 4. Representative ELN angular distributions for Cases A, B, and C (cf. Eq. 11 and Table I): $D_{\mathbf{p}}$ is represented by dashed lines and the effective $\tilde{D}_{\mathbf{p}}$ is plotted with solid lines. The inset highlights that there is an angular crossing in Case A, and its shape changes when beyond-mean-field corrections are taken into account, hence affecting the stability conditions.

els) and beyond-mean-field (bottom panels) scenarios. The linear growth rate of $|\rho_{ex}|_0$ agrees with the results from the normal mode analysis presented in Sec. III. Case A becomes unstable once the beyond-mean-field modifications are taken into account (note that the small oscillations visible on the top right panel are due to the initial seed). For Cases B and C, an overall smaller amount of flavor conversion takes place when beyond-mean-field corrections are taken into account.

In order to better grasp our findings in the non-linear regime, it is useful to express the density matrices in the orthonormal basis $\{1_{2 \times 2}, \sigma_x, \sigma_y, \sigma_z\}$, where $1_{2 \times 2}$ is the identity matrix and σ_i are the Pauli matrices: $\rho_{\mathbf{p}} = 1/2[\text{Tr}(\rho_{\mathbf{p}}) + \mathbf{P}_{\mathbf{p}} \cdot \boldsymbol{\sigma}]$. Thus, Eqs. (5) become:

$$i\hbar \frac{\partial \text{Tr}(\rho_{\mathbf{p}})}{\partial t} = 0, \quad (12a)$$

$$i\hbar \frac{\partial \mathbf{P}_{\mathbf{p}}}{\partial t} = \mu(\tilde{\mathbf{D}}_0 - v\tilde{\mathbf{D}}_1) \times \tilde{\mathbf{P}}_{\mathbf{p}}, \quad (12b)$$

and likewise for antineutrinos.

Coherent forward scattering, see Eq. (2), preserves the number of particles in each momentum mode, so $\text{Tr}(\rho_{\mathbf{p}})$ is conserved and flavor conversion is driven by $\mathbf{P}_{\mathbf{p}}$ and $\tilde{\mathbf{P}}_{\mathbf{p}}$. In the presence of neutrino-neutrino interactions, these polarization vectors do not evolve independently of each other. In the mean-field case, the behavior of the system can be described with a classical analogy: the dipole moment of the ensemble \mathbf{D}_1 acts like a gyroscopic pendulum, which precesses instantaneously around a time-dependent vector, $\dot{\mathbf{D}}_1 = \mu(\mathbf{D}_0 + \mathbf{D}_2) \times \mathbf{D}_1$. The monopole \mathbf{D}_0 plays the role of gravity and a linear combination of the multipoles mimics the angular momentum [16]. If the ELN distribution is stable, the pendulum is in the “sleeping top” configuration. If the ELN distribution is unstable, bipolar oscillations take place. This analogy does not hold when our prescription for neutrino degeneracy

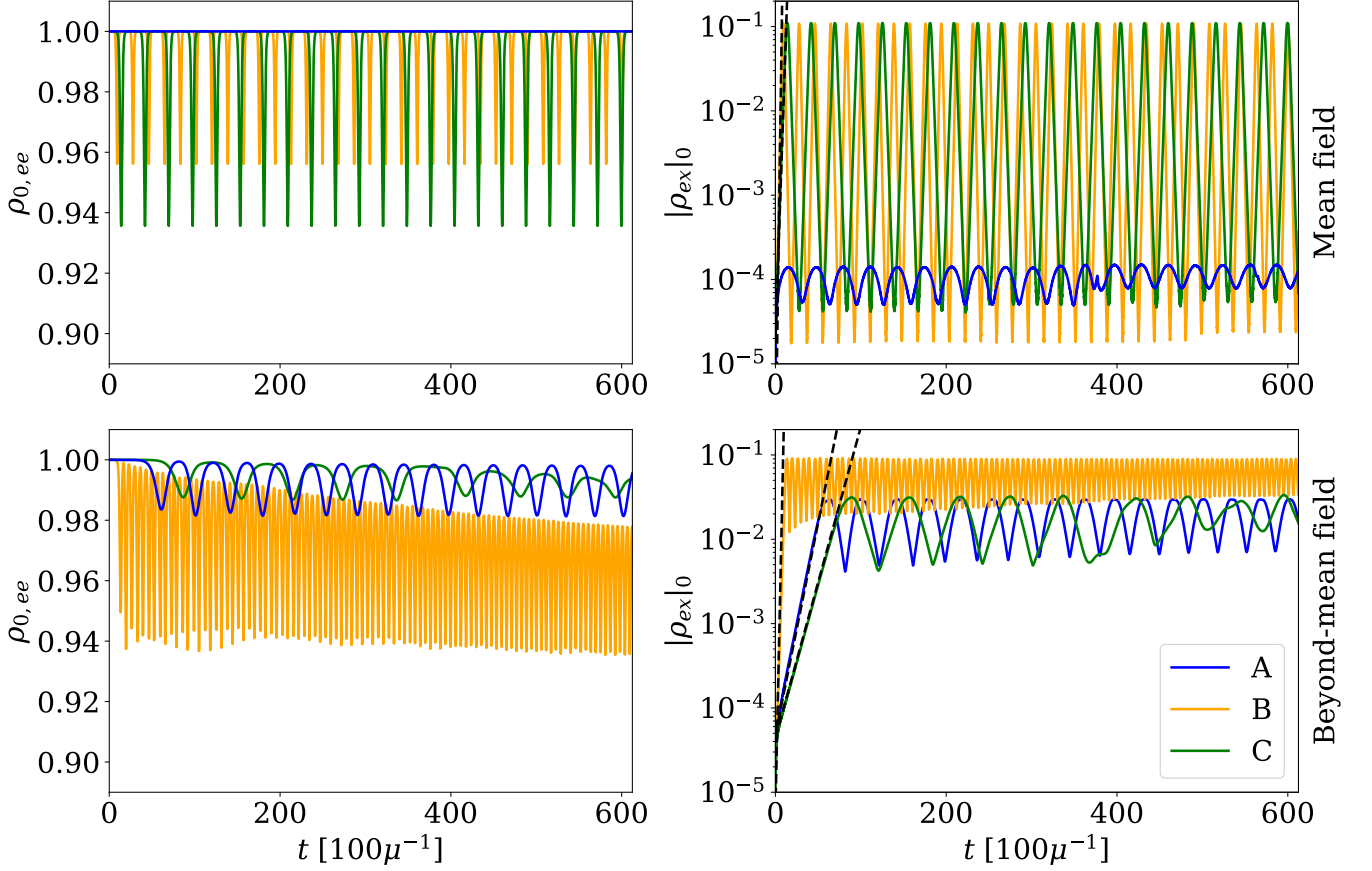


FIG. 5. Angle-integrated neutrino density (on the left) and flavor coherence (on the right) as functions of time for Cases A, B, and C (cf. Fig. 4 and Table I). The top panels have been obtained in the mean-field scenario, while the bottom panels represent the flavor outcome when beyond-mean-field effects due to neutrino degeneracy are taken into account. The results of the linear stability analysis are shown as dashed black lines. The beyond-mean-field terms are responsible for making Case A unstable, and damping flavor conversion for Cases B and C.

is included. As in the mean-field case, $\mathbf{P}_{\mathbf{p}}$ and $\bar{\mathbf{P}}_{\mathbf{p}}$ precess around a certain vector $\tilde{\mathbf{V}} \equiv \tilde{\mathbf{D}}_0 - v\tilde{\mathbf{D}}_1$. However, their x and y components are affected by the beyond-mean-field corrections. When the occupation numbers are low, the latter can be approximated using $(1 - B_l)^{1/2} \simeq 1 - 1/2B_l$:

$$i\hbar \frac{\partial P_{\mathbf{p};bl}^x}{\partial t} \simeq -\frac{\mu}{2} \tilde{V}^y (B_{e;\mathbf{p}} \rho_{ee;\mathbf{p}} - B_{x;\mathbf{p}} \rho_{xx;\mathbf{p}}), \quad (13a)$$

$$i\hbar \frac{\partial P_{\mathbf{p};bl}^y}{\partial t} \simeq +\frac{\mu}{2} \tilde{V}^x (B_{e;\mathbf{p}} \rho_{ee;\mathbf{p}} - B_{x;\mathbf{p}} \rho_{xx;\mathbf{p}}). \quad (13b)$$

Here, the upper indices denote the component of the vector in the Cartesian coordinate frame. The equations for antineutrinos are analogous. The terms in Eqs. (13) have two distinct effects in the non-linear regime of fast flavor conversion. Firstly, they change the length of $|\mathbf{P}_{\mathbf{p}}|$ and $|\bar{\mathbf{P}}_{\mathbf{p}}|$, and, if $B_{l;\mathbf{p}} \neq \bar{B}_{l;\mathbf{p}}$, also $|\mathbf{D}_1|$ —all of which are conserved in the mean-field case [16]. Secondly, they cause the evolution of the ensemble to become non-periodic. We show these results for our Case B in the top and bottom panels of Fig. 6, respectively.

The top panel of Fig. 6 describes the time evolution of $|\mathbf{D}_1|$, the length of the dipole vector. In principle, the violation of the conservation laws implies that the beyond-mean-field system should have more degrees of freedom than the mean-field one. However, the variation in $|\mathbf{D}_1|$ is small, because Eqs. (13) lead to subdominant effects with respect to the mean-field terms. Hence, the symmetries of the mean-field equation of motion are approximately respected. We have attempted to test this using the Gram matrix, which is defined as $G_{mn} = \int_{t_0}^{t_f} dt \mathbf{P}_{v_m}(t) \cdot \mathbf{P}_{v_n}(t)$ for an arbitrary time interval (t_0, t_f) [16, 46]. Here, v_n and v_m denote discrete angular modes. If the Gram matrix has rank N , the neutrino ensemble can be mapped into a system of N linearly independent beams. For the examples in Fig. 5, we find $N = 3$ in both the mean-field and beyond-mean-field cases. Thus, when our beyond-mean-field prescription is taken into account, the system retains a large degree of coherence, even though it does not behave like a gyroscopic pendulum.

The bottom panel of Fig. 6 depicts the evolution of the

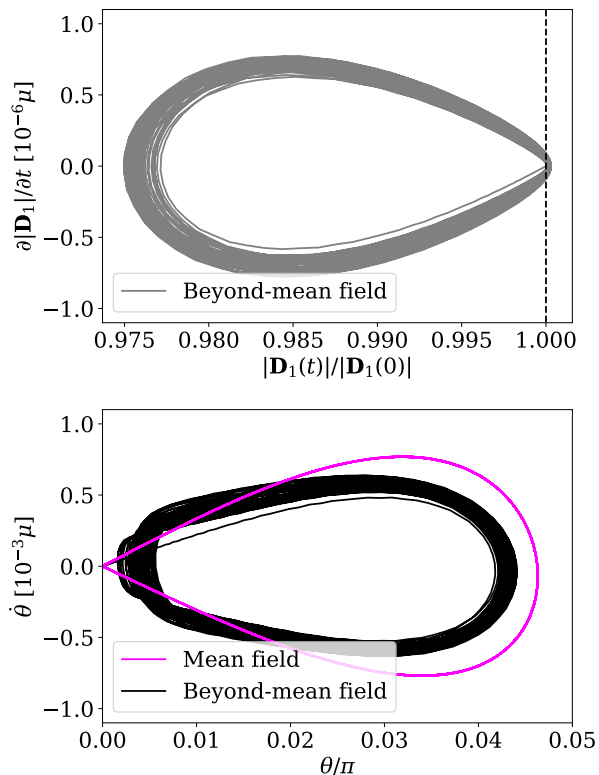


FIG. 6. Phase-space diagrams of $\mathbf{D}_1(t)$ for Case B. *Top panel:* The beyond-mean-field terms change the length of the dipole vector. *Bottom panel:* Flavor conversion in the beyond-mean field case is not periodic, and \mathbf{D}_1 tilts away from the flavor axis over time.

zenith angle $\theta \equiv \tan^{-1}(\sqrt{(D_1^x)^2 + (D_1^y)^2}/D_1^z)$. In both the mean-field and beyond-mean-field cases, the system starts in the upright position ($\theta = 0$). Then, in the mean-field case, flavor conversion creates a cyclic trajectory between $\theta = 0$ and a fixed endpoint, which depends on the shape of the angular distribution. On the contrary, in the scenario including beyond-mean-field modifications, the evolution is neither periodic nor bipolar. Over time, the interplay between the mean-field and the higher-order terms in Eq. (12b) causes the vector \mathbf{D}_1 to tilt away from the z -axis.

In general, the beyond-mean-field terms in Eqs. (13) are different for each $\mathbf{P}_{\mathbf{p}}$ and $\bar{\mathbf{P}}_{\mathbf{p}}$, since each polarization vector follows its own equation of motion. Adopting a decomposition in multipoles, e.g. $\mathbf{P}_{\mathbf{p}} = \sum_{n=0}^{\infty} (n + \frac{1}{2}) \mathbf{P}_n$, one can see a cascade of flavor instabilities towards ever smaller angular scales (cf. also Ref. [47]), which can be described as the growth of higher-order multipoles P_n^z and \bar{P}_n^z (see Fig. 7, left panels). As a visual aid, the right panels in Fig. 7 highlight the effect of the instability on the neutrino and antineutrino angular distributions for selected time snapshots in Case B. The top right panel shows the fast flavor pendulum: angular modes in the proximity of the ELN crossing evolve, undergoing synchronous oscillations. The bottom right panel shows

that, when beyond-mean-field corrections are included, flavor conversion begins around the ELN crossing, but spreads across angular modes.

We note that the equivalence between the $P_{\mathbf{p}}^z$ and $\bar{P}_{\mathbf{p}}^z$ equations of motion can be broken within the mean-field approximation. Indeed, if Eqs. (4) are extended to include vacuum oscillations, the $P_{n>0}^z$ and $\bar{P}_{n>0}^z$ multipoles also grow: see e.g. Ref. [48]. Incoherent scattering can also lead to a similar outcome, if the collision terms violate the symmetries of Eqs. (4): see e.g. Ref. [49]. For example, fast flavor instabilities cascade to small angular scales when the scattering terms are different for neutrinos and antineutrinos or, more generally, when they are energy-dependent. Even if the scattering rates are equal, collisions break the periodicity of flavor evolution, and cause a decrease in $|\mathbf{D}_1|$ [46, 50]. Hence, several different effects could lead to the same effective flavor outcome.

V. ENERGY-DEPENDENT FEATURES OF BEYOND-MEAN-FIELD EFFECTS

In order to investigate whether the beyond-mean-field corrections induce energy-dependent effects, we solve Eqs. (4) and (5) assuming Fermi-Dirac distributions for neutrinos and antineutrinos, with the initial distribution in Eq. (11). We consider $T = 10$ MeV, $\mu_{\nu_e} = 3$ MeV, and the same b and d as in Case B. For the sake of simplicity, we neglect vacuum mixing to highlight the effect of the beyond-mean-field corrections and generate flavor coherence by including a small off-diagonal perturbation in the initial conditions.

The left panel of Fig. 8 displays the energy- and angle-integrated (anti)neutrino distribution, P_0^z (\bar{P}_0^z), as a function of time. The mean-field system still behaves as a gyroscopic pendulum, because the self-interaction term is energy-independent. In the beyond-mean-field case, each polarization vector follows a different equation of motion, due to the additional terms in Eq. (13): hence, flavor evolution is no longer bipolar. Rather, each energy mode decoheres from the others, as shown in the right panel of Fig. 8. This means that beyond-mean-field terms can change the shape of the neutrino spectra, and the behavior of the multi-energy ensemble is intrinsically different from that of a single-energy approximation. However, the evolution of neutrinos and antineutrinos is still identical, which is a consequence of self-interactions conserving the ELN. Indeed, integrating over v and E in Eq. (12b) and the analogous expression for antineutrinos leads to $i\hbar\partial\mathbf{D}_0/\partial t = \mu(\bar{\mathbf{D}}_0 \times \mathbf{D}_0 - \mathbf{D}_1 \times \bar{\mathbf{D}}_1) = 0$.

VI. OUTLOOK

The physics of flavor conversion due to neutrino-neutrino interactions shows a very rich phenomenology that we are still far from fully grasping. Most of the existing work on this topic is carried out employing the

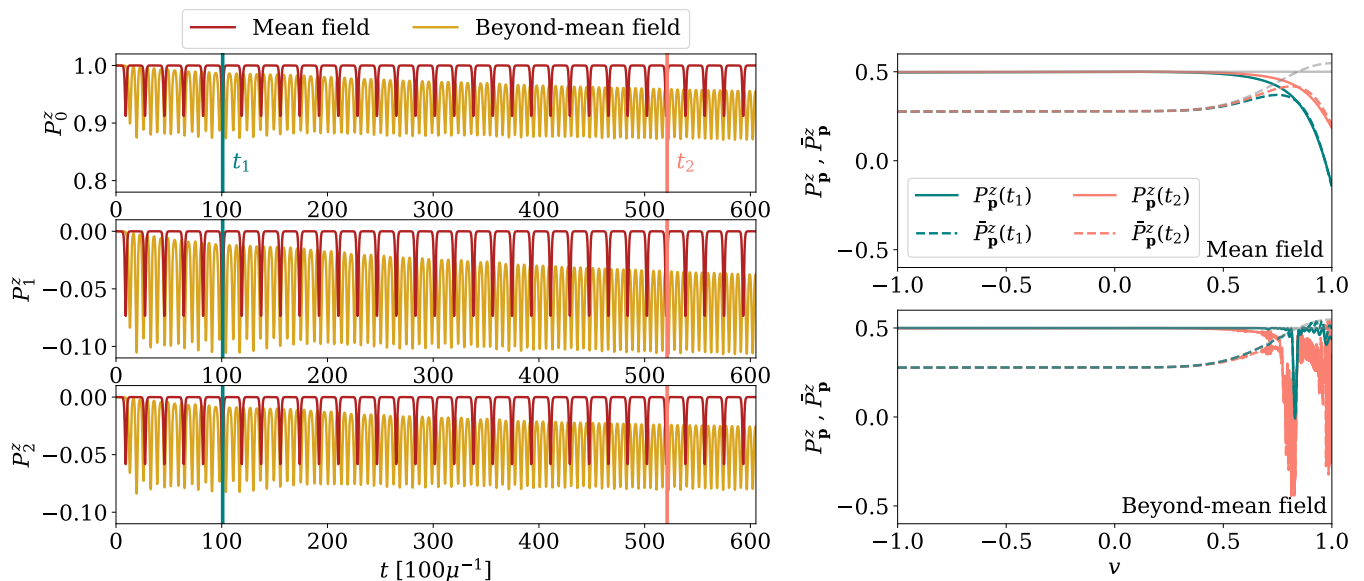


FIG. 7. *Left panels:* Time evolution of the multipoles of the neutrino angular distribution up to $n = 2$ for Case B. The average value of the multipoles evolves over time, reflecting the cascade of flavor waves towards smaller angular scales. The vertical lines mark the time snapshots shown in the right panels. *Right panels:* Angular distribution of the z component of the polarization vectors, P_p^z (solid) and \tilde{P}_p^z (dashed), for selected time snapshots in Case B. Gray lines mark the initial conditions. Flavor conversion spreads across angular modes in the case including beyond-mean-field terms, whereas it remains localized around the ELN crossing in the mean-field case.

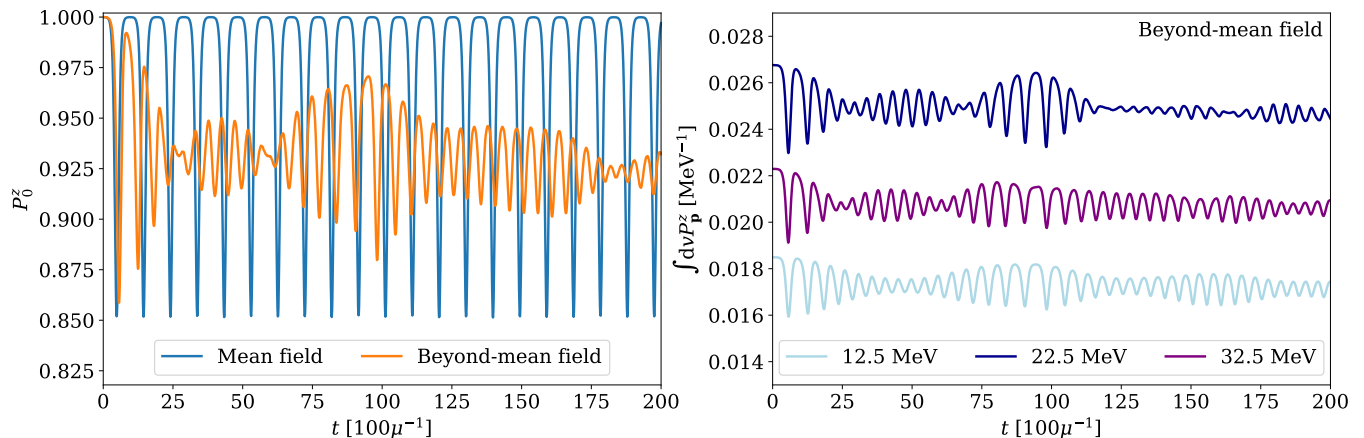


FIG. 8. *Left panel:* Monopole of the neutrino distribution as a function of time, for Case B. In the beyond-mean-field scenario, flavor conversion does not exhibit a bipolar behavior, due to the energy dependence of the additional terms in the equation of motion. *Right panel:* Time evolution of selected angle-integrated neutrino energy modes. Each polarization vector decoheres from the others, changing the shape of the energy spectrum.

mean-field approximation. In this paper, we have attempted to investigate whether beyond-mean-field effects on neutrino-neutrino coherent forward scattering could introduce flavor instabilities that are not otherwise foreseen. To this purpose, we have focused on the regime where neutrinos are degenerate and introduced a heuristic prescription for Pauli-blocking terms in the neutrino self-interaction Hamiltonian. Such corrections define an effective ELN distribution, which modifies the (anti)neutrino dispersion relation. Hence, ensembles that

are on the verge of stability in the mean-field case can become unstable when the beyond-mean-field terms are included and vice versa.

Relying on the gyroscopic pendulum analogy introduced for fast flavor conversion [16], we have investigated how the non-linear regime of the flavor evolution is modified by our beyond-mean-field prescription. Within the mean-field approximation, each (anti)neutrino polarization vector precesses around the potential generated by all other neutrinos in the ensemble. In the beyond-mean-

field scenario, additionally, the length of the polarization vectors changes due to dynamical decoherence. The terms that cause this effect introduce an energy dependence in the collective potential and break the symmetry between the neutrino and the antineutrino equations of motion. As a result, flavor instabilities cascade down to small angular scales, and the evolution of the system is not periodic anymore.

Qualitatively, the flavor conversion outcome including the beyond-mean-field effects in our toy model is similar to what observed when incoherent scattering and vacuum mixing are included in the mean-field equations of motion, although the physics linked to each of these phenomena and their interplay with the self-interaction term in the Hamiltonian is different. We have neglected these additional terms in the equations of motion throughout this work, to highlight the impact of beyond-mean-field corrections on fast instabilities. However, collisions, vacuum mixing, and potential beyond-mean-field corrections (due to momentum correlations caused by neutrino degeneracy) should coexist in the core of an astrophysical

system.

ACKNOWLEDGMENTS

We are grateful to Georg Raffelt for useful discussions. This project has received support from the Villum Foundation (Project No. 13164), the Danmarks Frie Forskningsfond (Project No. 8049-00038B), the European Union (ERC, ANET, Project No. 101087058), and the Deutsche Forschungsgemeinschaft through Sonderforschungsbereich SFB 1258 “Neutrinos and Dark Matter in Astro- and Particle Physics” (NDM). Views and opinions expressed are those of the authors only and do not necessarily reflect those of the European Union or the European Research Council. Neither the European Union nor the granting authority can be held responsible for them. The Tycho supercomputer hosted at the SCIENCE HPC Center at the University of Copenhagen was used for supporting the numerical simulations presented in this work.

-
- [1] L. Wolfenstein, Neutrino Oscillations in Matter, *Phys. Rev. D* **17**, 2369 (1978).
- [2] S. P. Mikheyev and A. Y. Smirnov, Resonance Amplification of Oscillations in Matter and Spectroscopy of Solar Neutrinos, *Sov. J. Nucl. Phys.* **42**, 913 (1985).
- [3] S. P. Mikheev and A. Y. Smirnov, Neutrino Oscillations in a Variable Density Medium and Neutrino Bursts Due to the Gravitational Collapse of Stars, *Sov. Phys. JETP* **64**, 4 (1986), arXiv:0706.0454 [hep-ph].
- [4] J. T. Pantaleone, Neutrino oscillations at high densities, *Phys. Lett. B* **287**, 128 (1992).
- [5] G. Sigl and G. G. Raffelt, General kinetic description of relativistic mixed neutrinos, *Nucl. Phys. B* **406**, 423 (1993).
- [6] A. Mirizzi and P. D. Serpico, Instability in the Dense Supernova Neutrino Gas with Flavor-Dependent Angular Distributions, *Phys. Rev. Lett.* **108**, 231102 (2012), arXiv:1110.0022 [hep-ph].
- [7] I. Tamborra and S. Shalgar, New Developments in Flavor Evolution of a Dense Neutrino Gas, *Ann. Rev. Nucl. Part. Sci.* **71**, 165 (2021), arXiv:2011.01948 [astro-ph.HE].
- [8] S. Richers and M. Sen, Fast Flavor Transformations, in *Handbook of Nuclear Physics*, edited by I. Tanihata, H. Toki, and T. Kajino (2022) pp. 1–17, arXiv:2207.03561 [astro-ph.HE].
- [9] M. C. Volpe, Neutrinos from dense environments: Flavor mechanisms, theoretical approaches, observations, and new directions, *Rev. Mod. Phys.* **96**, 025004 (2024), arXiv:2301.11814 [hep-ph].
- [10] I. Tamborra, Neutrinos from explosive transients at the dawn of multi-messenger astronomy, (2024), arXiv:2412.09699 [astro-ph.HE].
- [11] A. Banerjee, A. Dighe, and G. G. Raffelt, Linearized flavor-stability analysis of dense neutrino streams, *Phys. Rev. D* **84**, 053013 (2011), arXiv:1107.2308 [hep-ph].
- [12] S. Airen, F. Capozzi, S. Chakraborty, B. Dasgupta, G. G. Raffelt, and T. Stirner, Normal-mode Analysis for Collective Neutrino Oscillations, *JCAP* **12**, 019, arXiv:1809.09137 [hep-ph].
- [13] I. Izaguirre, G. G. Raffelt, and I. Tamborra, Fast Pairwise Conversion of Supernova Neutrinos: A Dispersion-Relation Approach, *Phys. Rev. Lett.* **118**, 021101 (2017), arXiv:1610.01612 [hep-ph].
- [14] S. Chakraborty, R. S. Hansen, I. Izaguirre, and G. G. Raffelt, Self-induced neutrino flavor conversion without flavor mixing, *JCAP* **03**, 042, arXiv:1602.00698 [hep-ph].
- [15] T. Morinaga, Fast neutrino flavor instability and neutrino flavor lepton number crossings, *Phys. Rev. D* **105**, L101301 (2022), arXiv:2103.15267 [hep-ph].
- [16] I. Padilla-Gay, I. Tamborra, and G. G. Raffelt, Neutrino Flavor Pendulum Reloaded: The Case of Fast Pairwise Conversion, *Phys. Rev. Lett.* **128**, 121102 (2022), arXiv:2109.14627 [astro-ph.HE].
- [17] D. F. G. Fiorillo and G. G. Raffelt, Slow and fast collective neutrino oscillations: Invariants and reciprocity, *Phys. Rev. D* **107**, 043024 (2023), arXiv:2301.09650 [hep-ph].
- [18] D. F. G. Fiorillo, M. Goimil-García, and G. G. Raffelt, Fast Flavor Pendulum: Instability Condition, (2024), arXiv:2412.09027 [hep-ph].
- [19] B. Dasgupta, Collective Neutrino Flavor Instability Requires a Crossing, *Phys. Rev. Lett.* **128**, 081102 (2022), arXiv:2110.00192 [hep-ph].
- [20] F. Capozzi, B. Dasgupta, E. Lisi, A. Marrone, and A. Mirizzi, Fast flavor conversions of supernova neutrinos: Classifying instabilities via dispersion relations, *Phys. Rev. D* **96**, 043016 (2017), arXiv:1706.03360 [hep-ph].
- [21] L. Johns, H. Nagakura, G. M. Fuller, and A. Burrows, Neutrino oscillations in supernovae: angular moments and fast instabilities, *Phys. Rev. D* **101**, 043009 (2020), arXiv:1910.05682 [hep-ph].
- [22] R. F. Sawyer, Speed-up of neutrino transformations in a supernova environment, *Phys. Rev. D* **72**, 045003 (2005),

- arXiv:hep-ph/0503013.
- [23] R. F. Sawyer, The multi-angle instability in dense neutrino systems, *Phys. Rev. D* **79**, 105003 (2009), arXiv:0803.4319 [astro-ph].
- [24] R. F. Sawyer, Neutrino cloud instabilities just above the neutrino sphere of a supernova, *Phys. Rev. Lett.* **116**, 081101 (2016), arXiv:1509.03323 [astro-ph.HE].
- [25] J. Ehring, S. Abbar, H.-T. Janka, G. G. Raffelt, and I. Tamborra, Fast neutrino flavor conversion in core-collapse supernovae: A parametric study in 1D models, *Phys. Rev. D* **107**, 103034 (2023), arXiv:2301.11938 [astro-ph.HE].
- [26] J. Ehring, S. Abbar, H.-T. Janka, G. G. Raffelt, and I. Tamborra, Fast Neutrino Flavor Conversions Can Help and Hinder Neutrino-Driven Explosions, *Phys. Rev. Lett.* **131**, 061401 (2023), arXiv:2305.11207 [astro-ph.HE].
- [27] H. Nagakura, Roles of Fast Neutrino-Flavor Conversion on the Neutrino-Heating Mechanism of Core-Collapse Supernova, *Phys. Rev. Lett.* **130**, 211401 (2023), arXiv:2301.10785 [astro-ph.HE].
- [28] M.-R. Wu, I. Tamborra, O. Just, and H.-T. Janka, Imprints of neutrino-pair flavor conversions on nucleosynthesis in ejecta from neutron-star merger remnants, *Phys. Rev. D* **96**, 123015 (2017), arXiv:1711.00477 [astro-ph.HE].
- [29] M. George, M.-R. Wu, I. Tamborra, R. Ardevol-Pulpillo, and H.-T. Janka, Fast neutrino flavor conversion, ejecta properties, and nucleosynthesis in newly-formed hypermassive remnants of neutron-star mergers, *Phys. Rev. D* **102**, 103015 (2020), arXiv:2009.04046 [astro-ph.HE].
- [30] O. Just, S. Abbar, M.-R. Wu, I. Tamborra, H.-T. Janka, and F. Capozzi, Fast neutrino conversion in hydrodynamic simulations of neutrino-cooled accretion disks, *Phys. Rev. D* **105**, 083024 (2022), arXiv:2203.16559 [astro-ph.HE].
- [31] R. Fernández, S. Richers, N. Mulyk, and S. Fahlman, Fast flavor instability in hypermassive neutron star disk outflows, *Phys. Rev. D* **106**, 103003 (2022), arXiv:2207.10680 [astro-ph.HE].
- [32] X. Li and D. M. Siegel, Neutrino Fast Flavor Conversions in Neutron-Star Postmerger Accretion Disks, *Phys. Rev. Lett.* **126**, 251101 (2021), arXiv:2103.02616 [astro-ph.HE].
- [33] D. F. G. Fiorillo, G. G. Raffelt, and G. Sigl, Inhomogeneous Kinetic Equation for Mixed Neutrinos: Tracing the Missing Energy, *Phys. Rev. Lett.* **133**, 021002 (2024), arXiv:2401.05278 [hep-ph].
- [34] A. V. Patwardhan, M. J. Cervia, E. Rrapaj, P. Siwach, and A. B. Balantekin, Many-Body Collective Neutrino Oscillations: Recent Developments, in *Handbook of Nuclear Physics*, edited by I. Tanihata, H. Toki, and T. Kajino (2023) pp. 1–16, arXiv:2301.00342 [hep-ph].
- [35] S. Shalgar and I. Tamborra, Do we have enough evidence to invalidate the mean-field approximation adopted to model collective neutrino oscillations?, *Phys. Rev. D* **107**, 123004 (2023), arXiv:2304.13050 [astro-ph.HE].
- [36] L. Johns, Neutrino many-body correlations, *Int. J. Mod. Phys. A* **39**, 2450122 (2024), arXiv:2305.04916 [hep-ph].
- [37] I. Tamborra, L. Huedepohl, G. G. Raffelt, and H.-T. Janka, Flavor-dependent neutrino angular distribution in core-collapse supernovae, *Astrophys. J.* **839**, 132 (2017), arXiv:1702.00060 [astro-ph.HE].
- [38] T. D. Brandt, A. Burrows, C. D. Ott, and E. Livne, Results From Core-Collapse Simulations with Multi-Dimensional, Multi-Angle Neutrino Transport, *Astrophys. J.* **728**, 8 (2011), arXiv:1009.4654 [astro-ph.HE].
- [39] S. Shalgar and I. Tamborra, On the Occurrence of Crossings Between the Angular Distributions of Electron Neutrinos and Antineutrinos in the Supernova Core, *Astrophys. J.* **883**, 80 (2019), arXiv:1904.07236 [astro-ph.HE].
- [40] T. Stirner, G. Sigl, and G. G. Raffelt, Liouville term for neutrinos: Flavor structure and wave interpretation, *JCAP* **05**, 016, arXiv:1803.04693 [hep-ph].
- [41] C. Volpe, D. Väänänen, and C. Espinoza, Extended evolution equations for neutrino propagation in astrophysical and cosmological environments, *Phys. Rev. D* **87**, 113010 (2013), arXiv:1302.2374 [hep-ph].
- [42] M. A. Rudzskii, Kinetic equations for neutrino spin- and type-oscillations in a medium, *Astrophys. Sp. Sci.* **165**, 65 (1990).
- [43] D. F. G. Fiorillo and G. G. Raffelt, Theory of neutrino fast flavor evolution. Part I. Linear response theory and stability conditions., *JHEP* **08**, 225, arXiv:2406.06708 [hep-ph].
- [44] P. Dedin Neto, I. Tamborra, and S. Shalgar, Energy Dependence of Flavor Instabilities Stemming from Crossings in the Neutrino Flavor Lepton Number Angular Distribution, (2023), arXiv:2312.06556 [astro-ph.HE].
- [45] D. F. G. Fiorillo and G. G. Raffelt, Flavor solitons in dense neutrino gases, *Phys. Rev. D* **107**, 123024 (2023), arXiv:2303.12143 [hep-ph].
- [46] G. G. Raffelt, N-mode coherence in collective neutrino oscillations, *Phys. Rev. D* **83**, 105022 (2011), [Erratum: *Phys.Rev.D* 104, 089902 (2021)], arXiv:1103.2891 [hep-ph].
- [47] L. Johns, H. Nagakura, G. M. Fuller, and A. Burrows, Fast oscillations, collisionless relaxation, and spurious evolution of supernova neutrino flavor, *Phys. Rev. D* **102**, 103017 (2020), arXiv:2009.09024 [hep-ph].
- [48] S. Shalgar and I. Tamborra, Dispelling a myth on dense neutrino media: fast pairwise conversions depend on energy, *JCAP* **01**, 014, arXiv:2007.07926 [astro-ph.HE].
- [49] S. Shalgar and I. Tamborra, A change of direction in pairwise neutrino conversion physics: The effect of collisions, *Phys. Rev. D* **103**, 063002 (2021), arXiv:2011.00004 [astro-ph.HE].
- [50] I. Padilla-Gay, I. Tamborra, and G. G. Raffelt, Neutrino fast flavor pendulum. II. Collisional damping, *Phys. Rev. D* **106**, 103031 (2022), arXiv:2209.11235 [hep-ph].